

MEDICAL SAM 2: SEGMENT MEDICAL IMAGES AS VIDEO VIA SEGMENT ANYTHING MODEL 2

Jiayuan Zhu
University of Oxford
jiayuan.zhu@ieee.org

Yunli Qi
University of Oxford

Junde Wu
University of Oxford
jundewu@ieee.org

ABSTRACT

In this paper, we introduce Medical SAM 2 (MedSAM-2), an advanced segmentation model that utilizes the SAM 2 framework to address both 2D and 3D medical image segmentation tasks. By adopting the philosophy of taking medical images as videos, MedSAM-2 not only applies to 3D medical images but also unlocks new One-prompt Segmentation capability. That allows users to provide a prompt for just one or a specific image targeting an object, after which the model can autonomously segment the same type of object in all subsequent images, regardless of temporal relationships between the images. We evaluated MedSAM-2 across a variety of medical imaging modalities, including abdominal organs, optic discs, brain tumors, thyroid nodules, and skin lesions, comparing it against state-of-the-art models in both traditional and interactive segmentation settings. Our findings show that MedSAM-2 not only surpasses existing models in performance but also exhibits superior generalization across a range of medical image segmentation tasks. Our code will be released at: <https://github.com/MedicineToken/Medical-SAM2>

1 INTRODUCTION

Large foundation models have demonstrated significant potential across various applications due to their robust zero-shot capabilities Wei et al. (2022); Kirillov et al. (2023); Wang et al. (2023b;a). Specifically, in the realm of medical image segmentation, the Segment Anything Model (SAM) Kirillov et al. (2023) has achieved remarkable success in zero-shot image segmentation tasks. Building upon the foundation laid by SAM, the enhanced Meta Segment Anything Model, SAM 2 Ravi et al. (2024), has recently been introduced as a cutting-edge, real-time object segmentation model applicable to both still images and video streams. This unified approach significantly diminishes user interaction time and elevates performance in video segmentation. Equipped with real-time processing capabilities and adept at managing complex scenarios involving object motion and occlusion, SAM 2 is poised to transform object segmentation practices in a variety of fields.

As a critical and unique component of visual segmentation, medical image segmentation entails partitioning an image into distinct regions of interest. This process is essential for applications such as diagnosis and image-guided surgery. Recently, automated segmentation methods have garnered attention due to their ability to improve both consistency and accuracy Wu et al. (2022b; 2023; 2024). The progression of deep learning techniques has facilitated the successful deployment of neural network-based models in medical image segmentation tasks. These models include the traditional convolutional neural networks (CNNs) as well as the more recently developed vision transformers (ViTs).

One significant challenge in medical image segmentation is model generalization. Specifically, a model trained on a particular target, such as an organ or tissue, cannot easily adapt to other targets. Consequently, unique models are typically required for each segmentation target. Previous efforts to address this include adopting the interactive segmentation paradigm Wu et al. (2023); Cheng et al. (2023a); Ma & Wang (2023), where, for example, a user can click on the desired organ, and the model will predict its segmentation even without prior training on that specific organ. However, this approach necessitates that the user provides a prompt for each image, which can be quite exhausting. Another distinct challenge in medical image segmentation is that many standard deep learning architectures developed for computer vision are designed for 2D images. However, in medical imaging, data often

exist in 3D formats, such as CT, MRI, and ultrasound images. This discrepancy creates a significant gap when applying general computer vision models to 3D medical imaging data.

In this work, we demonstrate that SAM 2, originally proposed as a general visual model for image and video segmentation, can be uniquely adapted to address these two significant challenges in medical image segmentation. The adaptation has led to the development of a highly effective model for medical image segmentation, termed Medical SAM 2 (MedSAM-2). Specifically, we adopt the high-level concept of treating medical images as videos, and we have designed a unique module along with a training and inference pipeline that enables SAM 2 to be applicable for both 2D and 3D medical image segmentation. As a result, the model not only achieves superior performance on 3D images but also unlocks a capability termed One-prompt Segmentation Wu & Xu (2024), which previous models have struggled to handle. In this scenario, users only need to provide a prompt for the first or a specific frame targeting an area, such as the optic cup in a fundus image. Subsequently, the model can autonomously segment the optic cup in subsequent images, even in the absence of temporal relationships between these images. This challenging setting, which has not been effectively addressed by nearly any existing model, is adeptly handled by MedSAM-2, which we refer to as capable of managing this one-prompt segmentation setting. Despite the complexity One-prompt Segmentation, this approach is extremely beneficial for clinical applications. When analyzing multiple images, clinicians need only select the first frame as the prompt, and the desired region will be automatically segmented in all subsequent frames without the need for further input. This significantly reduces the clinician’s effort. Furthermore, MedSAM-2 is a universal model capable of segmenting any object in any image, a feature often referred to as zero-shot generalization. This means it can be applied to visually new content without requiring custom adaptations. Additionally, MedSAM-2 offers significant flexibility to users, allowing them to refine the segmentation target at any time and on any frame while the model processes the data. This flexibility greatly enhances convenience for clinicians during medical image analysis.

We evaluated MedSAM-2 across 15 different benchmarks, encompassing 26 distinct tasks for validation. Compared with previous fully-supervised segmentation models and SAM-based interactive models, MedSAM-2 demonstrated superior performance across all tested methods and achieved state-of-the-art results in both 2D and 3D medical image segmentation tasks. Specifically, under the one-prompt segmentation setting, MedSAM-2 outperformed all previous few-shot and one-shot segmentation models, thereby showcasing its exceptional generalization capabilities.

In summary, our contributions are as follows:

1. We are the first to introduce a SAM-2 based medical image segmentation model, MedSAM-2.
2. We adopt a novel medical-images-as-videos philosophy, which inspired us to design a unique pipeline that unlock the One-prompt Segmentation capability in MedSAM-2, a feature scarcely achievable by previous methods.
3. We develop the unique modules and pipeline, incorporating confidence memory bank and weighted pick-up, to technically facilitate this capability.
4. We evaluate MedSAM-2 across 15 different benchmarks, including 26 distinct tasks, where the model achieves superior performance.

2 METHOD

SAM 2 has recently been introduced as a universal model for high-performance image and video segmentation. By treating medical images as videos and design a unique pipeline following this philosophy, we enhanced 3D medical image segmentation performance and unlocked a unique one-prompt segmentation capability. We have named this innovative model MedSAM-2. In the sections that follow, we discuss our motivations for applying MedSAM-2 to 3D medical images in Section 2.1, our rationale for its use with 2D medical images in Section 2.1, our novel module and pipeline in Section 2.3, and provide a brief overview of the model architecture in Section 2.4.

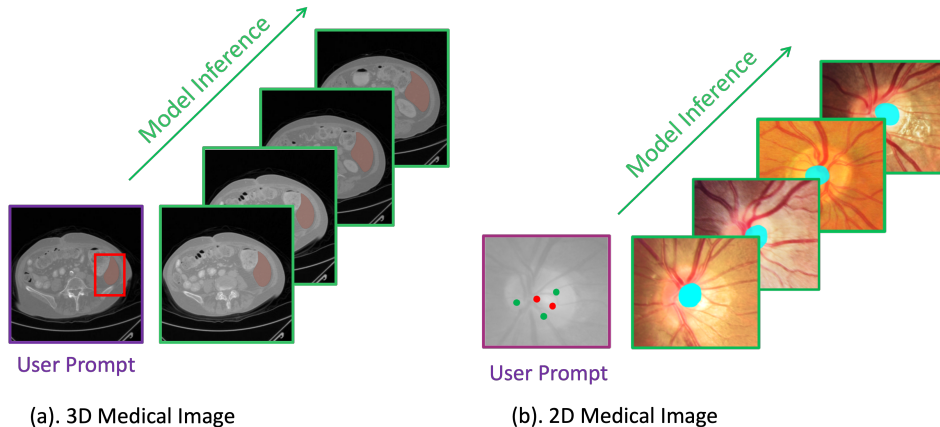


Figure 1: An illustration showcasing the capability of MedSAM-2. When provided with a prompt in one 3D slice, MedSAM-2 can segment all later spatial-temporal 3D frames. When given a prompt in one 2D image, MedSAM-2 can accurately segment other 2D images that are not temporally related using the same criteria, which is an emergence of One-prompt Segmentation capability.

2.1 APPLYING SAM 2 ON 3D MEDICAL IMAGES

A straightforward approach to processing 3D medical images involves treating them as sequences of 2D slices. However, the intrinsic associations between sequential slices can be leveraged to address numerous challenges encountered in single-slice 2D image processing. For instance, organs or tissues in medical images may display blurry boundaries due to patient or medical device movement. Utilizing the contextual information from adjacent slices can enable accurate segmentation of a slice, even if its quality is compromised.

SAM 2, a pre-trained foundational network for video segmentation, is adept at processing 3D video data and is designed to track and segment objects across video frames. Thus, it is straightforward to utilize such a model for 3D medical images. The contiguous nature of 3D medical images resembles that of natural videos—not only in dimensions but also in the high association between frames. This similarity allows SAM 2 to track and enhance the segmentation of a target throughout the entire 3D image without requiring additional prompts for each slice.

2.2 FROM UNIVERSAL IVOS TO ONE-PROMPT SEGMENTATION

Although the adoption of SAM 2 for 3D medical imaging is straightforward, its unique advantages for 2D image segmentation, beyond its inherent segmentation capabilities, are not immediately apparent. However, we discovered that when a set of 2D medical images—each containing the same type of organ but differing in content and lacking temporal connections—is treated as a video sequence, SAM 2 can unlock a ‘One-prompt Segmentation’ capability rarely achieved by other methods.

One-prompt Segmentation, as previously defined in Wu & Xu (2024), is a method where, for an unseen example, the user needs only to provide *one prompted sample* to the trained model. The model then performs effectively on this task without requiring any retraining or fine-tuning, thanks to its generalization capabilities. In this paper, we argue that transferring the video segmentation capabilities of SAM 2 to process 2D image sequences is an effective approach to achieving one-prompt segmentation. To conceptualize formally:

Consider a set \mathcal{S} encompassing a wide range of different medical image segmentation tasks. Each task s is annotated as image and label pairs $\{x_s, y_s\}$. Fully-supervised segmentation methods typically would learn a function $y_s = f_\theta^d(x_s)$ to estimate a segmentation map y_s from an input image x_s . However, this function f_θ^s is specific to the task s .

In the case of universal interactive video object segmentation (iVOS), then its target is to learn a universal function $y^k = f_\theta(x_u^k, P_u)$, that y^k and x^k means the sequential video frames in the time

order, x_u^k means the image contains the unseen object u , and P_u is a set of prompts on the target unseen object u , to hint the model generalize to u on any possible x that contain the object. The prompt in the set could have the association relationship that multiple prompts is for one specific image, and multiple images can be prompted.

On the other side, in One-Prompt Segmentation setting, approach learns a general function $y = f_\theta(x_s, t_s)$ applicable to any medical task s . Here, $t_s = \{x_{s_c}, p_{s_c}\}$ consists of a fixed template image x_{s_c} and an associated prompt p_{s_c} . If we consider in iVOS, the video that contains the unseen object as the new task in task set \mathcal{S} , then we have $y^k = f_\theta(x_s^k, P_s)$ in iVOS. Comparing this with the function of One-Prompt Segmentation, it becomes apparent that One-Prompt Segmentation is analogous to iVOS under the following two conditions:

1. The image-label pair in iVOS is not strictly sequential, allowing One-Prompt Segmentation to segment the same object across different images even if they lack a temporal relationship.
2. The prompt in iVOS is limited to just one, applied to a random image in the processed image set. Consequently, the transition between iVOS and One-Prompt Segmentation is straightforward when a set of images containing the same object is treated as a video sequence.

Although the two paradigms may appear technologically similar, they have different significance in various applications. The One-Prompt paradigm is particularly user-friendly in clinical settings, as it requires only a single sample with prompts, enabling the model to adapt to new tasks in a single forward pass. This simplicity offers a significant advantage for clinicians without a computer science background, as it eliminates the need for complex training or fine-tuning processes.

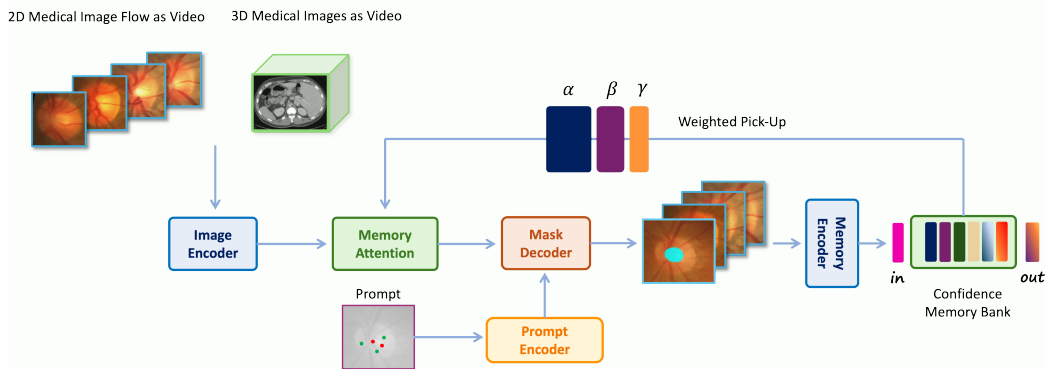


Figure 2: MedSAM-2 Framework: Building on the SAM 2 framework, we propose treating 3D medical images and 2D medical image flows as videos to facilitate memory-enhanced medical image segmentation. This approach not only improves performance in 3D medical image segmentation but also unlock One-Prompt Segmentation capability for 2D medical image flows. This is achieved by incorporating our proposed Confidence Memory Bank and Weighted Pick-up strategy.

2.3 SEGMENT MEDICAL IMAGES AS VIDEOS

As we recognize the inherent similarity between video segmentation and the medical one-prompt segmentation paradigm, we adapt SAM 2—a well-designed video segmentation model—for medical image segmentation by treating medical images as videos. We have developed two distinct running pipelines for 3D and 2D medical images, respectively. We begin by discussing the simpler 3D medical image pipeline.

Processing 3D medical images in the SAM 2 model is largely analogous to processing video data, given the strong temporal association between neighboring slices in the 3D medical images. Specifically, we utilize the memory system originally employed in SAM 2 to retrieve previous slices and their corresponding predictions for sequential slice segmentation. The core concept involves conditioning the frame embeddings, post-image encoder, with memories of past predictions and prompted frames. These memories, encoded by a neural network-based memory encoder, are stored in a memory bank acting as a buffer region. During the conditioning process, the input image embedding

is enhanced by the memory embedding via a memory attention operation, predominantly based on the transformer attention mechanism. Once the input embedding is conditioned with the memory feature through memory attention, it is forwarded to the decoder to predict the segmentation. The segmentation results are then added back to the memory bank to assist in tracking the segmentation of subsequent slices.

We approach the processing of 2D medical images differently from SAM 2 to enable the one-prompt capability of MedSAM-2. Initially, we group a set of medical images containing the same organ or tissue into what we call a 'medical image flow'. Although these images lack a temporal relationship, we treat the flow as a video sequence for segmentation purposes. Our objective is that once a user prompts a random image in this flow, MedSAM-2 will not only predict the segmentation for that image but also propagate this prediction to all other images in the flow. To achieve this, we employ a unique memory mechanism.

Unlike the temporal first-in-first-out queue used in SAM 2, we introduce a 'confidence-first' memory bank to store templates for the model. Specifically, during the inference stage, MedSAM-2 stores the results it is most confident about in a first-in-first-out queue within the memory bank, alongside the prompted templates. Confidence is calculated based on the probability of the model's predictions. This method ensures that the templates in the memory bank are the most accurate samples the model recognizes, thus minimizing the impact of noisy templates. We also implement an image diversity constraint when adding images to the bank, ensuring that the memory encompasses a wide variety of images to better match incoming input images; this diversity is assessed through the similarity of image embeddings.

When merging an input image embedding with information from the memory bank, we diverge from the SAM 2 approach of equally merging all information. Instead, we employ a weighted pick-up strategy, assigning higher weights to images more similar to the input image to facilitate easier propagation. During the training stage, we use a calibration head Ji et al. (2021) to ensure that the model predicts more accurate segmentations with higher confidence and less accurate segmentations with lower confidence. This calibration aligns the model's confidence with the accuracy of its predictions, thus enhancing the effectiveness of the confidence memory bank.

2.4 MEDSAM-2 ARCHITECTURE

Med-SAM2 features an image encoder that abstracts the input into embeddings, a memory encoder that abstracts predicted frame embeddings, and a memory attention mechanism to condition the input embedding with memories stored in the memory bank. The basic architecture is similar to that used in SAM 2 Ravi et al. (2024). For readers unfamiliar with this architecture, we provide a brief introduction to each component.

The encoder and decoder in the network bear resemblance to those in SAM Roy et al. (2023). The encoder consists of a hierarchical vision transformer, and the decoder comprises a lightweight bi-directional transformer that integrates prompt embeddings with image embeddings. The prompt embeddings are generated by a prompt encoder, which processes the user's prompt to abstract the corresponding embedding.

The memory attention component consists of a series of stacked attention blocks, each incorporating self-attention blocks followed by a cross-attention mechanism. This structure integrates memories of frames and object pointers stored in a memory bank. The object pointers are comprised of a series of vectors that represent the semantic information of the object to be segmented, derived from the mask decoder output tokens of each frame. This architecture allows users to prompt any frame during the 3D image segmentation process, as the memory attention mechanism incorporates user-provided intermediate prompts to refine the segmentation results.

3 EXPERIMENT

3.1 DATASET

We initiated our study by conducting experiments on five distinct medical image segmentation datasets, using auto-generated mask prompts. These datasets fall into two categories. The first

category aims to evaluate general segmentation performance, for which we selected the abdominal multi-organ segmentation task. This task poses one of the most significant challenges in the field, and we utilized the BTCV dataset Fang & Yan (2020), a widely recognized and publicly available benchmark that includes twelve anatomical structures.

The remaining four datasets were chosen to assess the model’s ability to generalize across different imaging modalities. These included optic disc and optic cup segmentation on fundus images, using the REFUGE2 dataset Fang et al. (2022); brain tumor segmentation on MRI scans, using the BraTs 2021 dataset Baid et al. (2021); thyroid nodule segmentation on ultrasound images, using the TNMIX benchmark, which combines 4554 images from TNSCUI Ma et al. (2017) with 637 images from DDTI Pedraza et al. (2015); and melanoma or nevus segmentation on dermoscopic images, using the ISIC 2019 dataset Milton (2019).

We further evaluated the model’s one-prompt segmentation performance using 10 additional 2D image segmentation tasks, with different types of prompts. Specifically, the KiTS23Heller et al. (2023), ATLAS23Quinton et al. (2023), TDSCTds (20203), and WBCZheng et al. (2018) datasets employed the *point* prompt technique. For the SegRap Astaraki et al. (2023), CrossM23 Cro (2023), and REFUGE Fang et al. (2022) datasets, we utilized the *BBox* (bounding box) prompt. Lastly, the *mask* prompt was applied to the CadVidSet Wang et al. (2020), STAR Hoover et al. (2000), and ToothFairy Bolelli (2023) datasets.

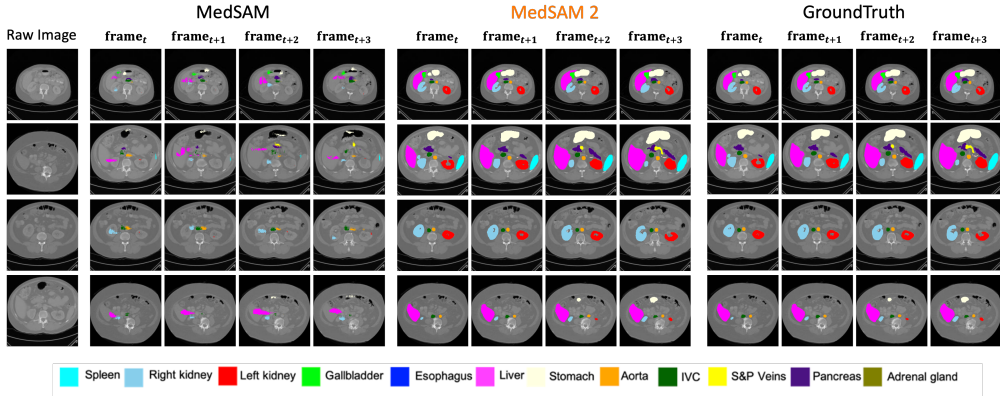


Figure 3: Comparison of MedSAM, MedSAM-2, and ground truth on sequential 3D medical image segmentation.

3.2 EVALUATION METRICS

We use Intersection over Union (IoU) and Dice Score to assess the performance of models in medical image segmentation.

Intersection over Union (IoU) Intersection over Union (IoU), also known as the Jaccard Index, is a measure used to evaluate the accuracy of an object detector on a specific dataset. It quantifies the overlap between two datasets by dividing the area of overlap between the predicted segmentation and the ground truth by the area of their union. The formula for IoU is given by:

$$\text{IoU} = \frac{\text{Area of Overlap}}{\text{Area of Union}}$$

IoU provides a clear metric at the object level, assessing both the size and position accuracy of the prediction relative to the actual data, which is particularly useful for understanding detection model performance.

Dice Score The Dice Score, or Dice Coefficient, is a statistical tool that compares the similarity between two samples. It is particularly prevalent in medical image analysis due to its sensitivity to the size of the objects being examined. The Dice Score is calculated by taking twice the area of overlap

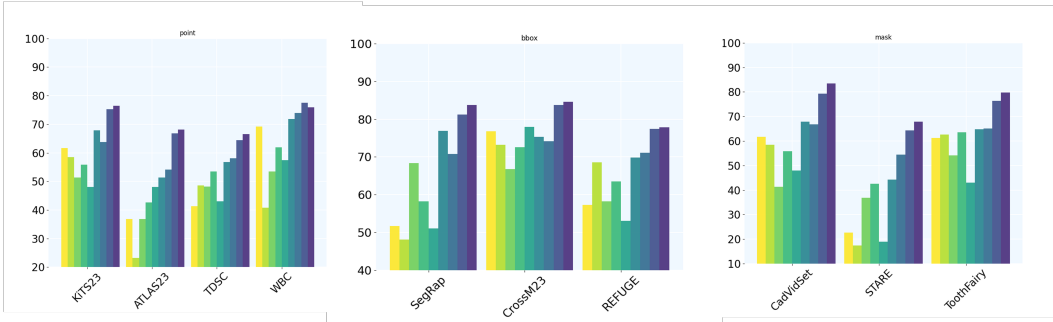


Figure 4: MedSAM-2 v.s. Few/One-shot Models under One-prompt Segmentation setting on 10 datasets with different prompts.

between the predicted and actual segmentations, divided by the total number of pixels in both the prediction and the ground truth. The formula for the Dice Score is:

$$\text{Dice Score} = \frac{2 \times \text{Area of Overlap}}{\text{Area of Prediction} + \text{Area of Ground Truth}}$$

This score ranges from 0 to 1, where a score of 1 indicates perfect agreement between the model’s predictions and the ground truth. The Dice Score is known for its robustness against the size variability of the segmented objects, making it extremely valuable in medical applications where such variability is common.

Both metrics, IoU and Dice Score, provide comprehensive insights into model accuracy, with Dice Score being particularly effective in scenarios involving significant variations in object size.

Hausdorff Distance (HD95) Metric The Hausdorff Distance (HD95) is a metric used to determine the extent of discrepancy between two sets of points, typically used to evaluate the accuracy of object boundaries in image segmentation tasks. It is particularly useful for quantifying the worst-case scenario of the distance between the predicted segmentation and the ground truth boundary.

The Hausdorff Distance measures the maximum distance of a set to the nearest point in the other set. For image segmentation, this means calculating the greatest of all the distances from a point in the predicted boundary to the closest point in the ground truth boundary and vice versa. The formula for the Hausdorff Distance is given by:

$$\text{HD} = \max \left(\sup_{x \in A} \inf_{y \in B} d(x, y), \sup_{y \in B} \inf_{x \in A} d(x, y) \right)$$

where A and B represent the sets of boundary points of the ground truth and the predicted segmentation, respectively, and $d(x, y)$ denotes the Euclidean distance between points x and y .

While the Hausdorff Distance provides a strict measure by considering the maximum distance, it can be overly sensitive to outliers. To mitigate this, the HD95 metric is used, which considers only the 95th percentile of the distances instead of the maximum. This adjustment makes the HD95 less sensitive to outliers and provides a more robust measure for practical applications:

$$\text{HD95} = 95\text{th percentile of } \{d(x, y) \mid x \in A, y \in B\}$$

This metric is particularly relevant in medical image analysis where precision in the segmentation of anatomical structures is critical and outliers can distort the evaluation of segmentation performance.

3.3 RESULTS

Note that the comparison presented may not be entirely fair due to undisclosed training details, such as data and implementation, for some models. Additionally, differences in model functionalities and intended application scenarios mean that many models cannot be compared on equal footing. Therefore, we treat these models primarily as references and focus more on presenting our approach for building a powerful medical image segmentation model.

3.3.1 PERFORMANCE OF UNIVERSAL MEDICAL IMAGE SEGMENTATION

In this section, we benchmark MedSAM-2 against a comprehensive array of state-of-the-art (SOTA) medical image segmentation methods, covering both 2D and 3D medical image segmentation tasks widely recognized within the community. For 3D medical images, prompts are provided randomly with a probability of 0.25, and for 2D images, the probability is 0.3. Initial results for 3D medical image segmentation are presented in Table 1, focusing on multi-organ segmentation tasks.

On 3D Medical Images To assess the general performance of our proposed model, we compare MedSAM-2 to established SOTA segmentation methods on the BTCV multi-organ segmentation dataset. The comparison includes renowned models such as nnUNet Isensee et al. (2021), TransUNet Chen et al. (2021), UNetr Hatamizadeh et al. (2022b), Swin-UNetr Hatamizadeh et al. (2022a), and diffusion-based models like EnsDiff Wolleb et al. (2021), SegDiff Amit et al. (2021), and MedSegDiff Wu et al. (2022b). Additionally, interactive segmentation models such as vanilla SAM, fully fine-tuned MedSAM Ma & Wang (2023), SAMed Zhang et al. (2023), SAM-Med2D Cheng et al. (2023b), SAM-U Deng et al. (2023), VMN Zhou et al. (2023) and FCFI Wei et al. (2023) are evaluated. For optimal performance in FCFI, ConvNext-v2-H Woo et al. (2023) serves as the backbone. Performance is quantified using the Dice score.

In the results presented in the table, MedSAM-2 demonstrates a significant advancement over previous models, MedSAM and SAM. Notably, on the BTCV dataset, MedSAM-2 sets a new state-of-the-art for multiple organ segmentation, achieving an overall superior performance. Specifically, MedSAM-2 reaches a final Dice score of 88.57%. This score not only surpasses the baseline zero-shot SAM-2 by a substantial 36.97%, but also exceeds the previous fully-supervised state-of-the-art, MedSegDiff, by a margin of 0.70%. Moreover, among interactive models, MedSAM-2 maintains the lead, outperforming the previously leading interactive model, Med-SA, by 2.78%. It is important to note that all these competing interactive models require prompts for each frame, whereas MedSAM-2 achieves better results with far fewer user prompts.

Table 1: The comparison of MedSAM-2 with SOTA segmentation methods over BTCV dataset evaluated by Dice Score.

Model	Spleen	R.Kid	L.Kid	Gall.	Eso.	Liver	Stom.	Aorta	IVC	Veins	Panc.	AG	Ave
TransUNet	0.952	0.927	0.929	0.662	0.757	0.969	0.889	0.920	0.833	0.791	0.775	0.637	0.838
UNetr	0.968	0.924	0.941	0.750	0.766	0.971	0.913	0.890	0.847	0.788	0.767	0.741	0.856
Swin-UNetr	0.971	0.936	0.943	0.794	0.773	0.975	0.921	0.892	0.853	0.812	0.794	0.765	0.869
nnUNet	0.942	0.894	0.910	0.704	0.723	0.948	0.824	0.877	0.782	0.720	0.680	0.616	0.802
EnsDiff	0.938	0.931	0.924	0.772	0.771	0.967	0.910	0.869	0.851	0.802	0.771	0.745	0.854
SegDiff	0.954	0.932	0.926	0.738	0.763	0.953	0.927	0.846	0.833	0.796	0.782	0.723	0.847
MedSegDiff	0.973	0.930	0.955	0.812	0.815	0.973	0.924	0.907	0.868	0.825	0.788	0.779	0.879
SAM	0.518	0.686	0.791	0.543	0.584	0.461	0.562	0.612	0.402	0.553	0.511	0.354	0.548
SAM 2	0.366	0.724	0.642	0.772	0.501	0.270	0.415	0.040	0.179	0.630	0.682	0.746	0.516
MedSAM	0.751	0.814	0.885	0.766	0.721	0.901	0.855	0.872	0.746	0.771	0.760	0.705	0.803
SAM-U	0.868	0.776	0.834	0.690	0.710	0.922	0.805	0.863	0.844	0.782	0.611	0.780	0.790
SAM-Med2D	0.873	0.884	0.932	0.795	0.790	0.943	0.889	0.872	0.796	0.813	0.779	0.797	0.847
SAMed	0.862	0.710	0.798	0.677	0.735	0.944	0.766	0.874	0.798	0.775	0.579	0.790	0.776
VMN	0.803	0.788	0.801	0.783	0.712	0.870	0.821	0.832	0.825	0.742	0.655	0.710	0.779
FCFI	0.876	0.834	0.889	0.795	0.781	0.945	0.887	0.921	0.897	0.829	0.780	0.760	0.858
MedSAM-2	0.918	0.924	0.921	0.927	0.913	0.836	0.874	0.894	0.838	0.838	0.832	0.901	0.886

On 2D Medical Images We also evaluate MedSAM-2 against state-of-the-art (SOTA) segmentation methods tailored for specific tasks across different image modalities, as detailed in Table 2. For optic cup segmentation, we compare with ResUnetYu et al. (2019) and BEALWang et al. (2019b); for brain tumor segmentation, with TransBTSWang et al. (2021b) and SwinBTSWang et al. (2021b); for thyroid nodule segmentation, with MTSegGong et al. (2021) and UltraUNetChu et al. (2021); and for skin lesion segmentation, with FAT-NetWu et al. (2022a) and BATWang et al. (2021a). Additionally, we benchmark against interactive models that require user prompts for each image.

The results from the table illustrate that MedSAM-2 outperforms all compared methods across five distinct tasks, showcasing its superior generalization across diverse medical segmentation tasks and image modalities. Specifically, MedSAM-2 achieves improvements of 2.0% on the Optic-Cup, 1.6% on Brain Tumor, and 2.8% on Thyroid Nodule, measured by the Dice score. Even against interactive models—which necessitate prompts for each image—MedSAM-2 maintains its lead, affirming the effectiveness of the proposed confidence memory bank in boosting performance.

Table 2: The comparison of MedSAM-2 with SOTA segmentation methods on different image modalities. The grey background denotes the methods are proposed for that/these particular tasks. Best results are denoted as **bold**.

		REFUGE2-Disc		REFUGE2-Cup		BraTs			TNMIX		ISIC	
		Dice	IoU	Dice	IoU	Dice	IoU	HD95	Dice	IoU	Dice	IoU
Optic Disc/Cup	ResUNet	92.9	85.5	80.1	72.3	78.4	71.3	18.71	78.3	70.7	87.1	78.2
	BEAL	93.7	86.1	83.5	74.1	78.8	71.7	18.53	78.6	71.6	86.6	78.0
Brain Tumor	TransBTS	94.1	87.2	85.4	75.7	87.6	78.44	12.44	83.8	75.5	88.1	80.6
	SwinBTS	95.2	87.7	85.7	75.9	88.7	81.2	10.03	84.5	76.1	89.8	82.4
Thyroid Nodule	MTSeg	90.3	83.6	82.3	73.1	82.2	74.5	15.74	82.3	75.2	87.5	79.7
	UltraUNet	91.5	82.8	83.1	73.8	84.5	76.3	14.03	84.5	76.2	89.0	81.8
Skin Lesion	FAT-Net	91.8	84.8	80.9	71.5	79.2	72.8	17.35	80.8	73.4	90.7	83.9
	BAT	92.3	85.8	82.0	73.2	79.6	73.5	15.49	81.7	74.2	91.2	84.3
General Med Seg	nnUNet	94.7	87.3	84.9	75.1	88.5	80.6	11.20	84.2	76.2	90.8	83.6
	TransUNet	95.0	87.7	85.6	75.9	86.6	79.0	13.74	83.5	75.1	89.4	82.2
	UNetr	94.9	87.5	83.2	73.3	87.3	80.6	12.81	81.7	73.5	89.7	82.8
	Swin-UNetr	95.3	87.9	84.3	74.5	88.4	81.8	11.36	83.5	74.8	90.2	83.1
Diffusion Based	EnsemDiff	94.3	87.8	84.2	74.4	88.7	80.9	10.85	83.9	75.3	88.2	80.7
	SegDiff	92.6	85.2	82.5	71.9	85.7	77.0	14.31	81.9	74.8	87.3	79.4
	MedsegDiff	95.1	87.6	85.9	76.2	88.9	81.2	10.41	84.8	76.4	91.3	84.1
SAM Based	SAM	-	-	-	-	63.2	47.6	32.53	-	-	81.6	70.4
	SAMed	89.9	81.8	80.7	70.8	77.3	68.8	19.07	78.9	71.2	87.4	78.9
	SAM-Med2D	92.1	83.7	82.0	75.3	82.9	74.1	16.20	80.3	73.6	87.8	78.3
	SAM-U	91.2	82.4	81.5	73.2	81.0	72.9	17.26	79.8	74.0	88.7	79.6
	VMN	92.5	83.9	82.8	76.1	83.4	74.6	17.13	81.4	74.2	88.3	79.1
	FCFI	95.5	88.3	85.7	77.7	87.0	78.2	12.32	84.3	75.7	89.6	81.5
	MedSAM	92.9	85.5	82.1	73.8	81.5	74.3	15.68	81.3	74.7	86.8	77.5
Med-SA	97.1	89.2	86.2	78.5	88.7	80.3	10.92	85.4	77.5	91.8	83.0	
Proposed	MedSAM-2	97.8	88.8	87.6	81.2	90.5	83.8	7.26	87.6	80.1	92.7	84.6

3.3.2 ONE-PROMPT SEGMENTATION PERFORMANCE UNDER DIFFERENT PROMPTS

We further assess MedSAM-2 under the One-Prompt segmentation setting by comparing it to various few/one-shot learning baselines that use different prompts. This experiment evaluates MedSAM-2’s performance in a challenging scenario where only one prompt is given, and there is no clear connection between sequential images.

We benchmark against several few-shot models—PANetWang et al. (2019a), ALPNetOuyang et al. (2020), SENetRoy et al. (2020), and UniverSegButoi et al. (2023)—all provided with the same template for consistency. For a fair comparison, all few-shot methods are given only one template with a prompt during testing. Additionally, we compare with one-shot models: DATZhao et al. (2019), ProbOne Ding et al. (2021), HyperSegNasPeng et al. (2022), and One-prompt Wu & Xu (2024). These models are trained on the same dataset as ours and receive segmentation labels as ‘prompts’ since they cannot utilize sparse prompts except One-prompt Wu & Xu (2024).

Figure 4 presents the average Dice scores per task for each method. Notably, the compared few/one-shot models require a mask as the prompt, giving them a potential advantage over our approach. Nevertheless, MedSAM-2 consistently outperforms these models by significant margins, demonstrating robust generalization across various tasks. Even when compared with the highly trained One-prompt Segmentation modelWu & Xu (2024), which was trained on 64 different medical datasets—far more than ours—MedSAM-2 still excels, outperforming it in 9 out of 10 tasks. In scenarios where all methods are provided with masks (as shown in Figure 4 mask), MedSAM-2 shows even more pronounced leads, typically surpassing the second-best by an average of 3.1%, the largest margin among all prompt settings.

4 CONCLUSION

In conclusion, MedSAM-2 represents a significant advancement model in the field of medical image segmentation. By integrating the SAM 2 framework and adopting a video-like approach to medical image processing, MedSAM-2 successfully extends the application of advanced segmentation techniques to both 2D and 3D medical images. The emergent ability of One-prompt segmentation has notably reduced the need for continuous user interaction, facilitating a more efficient and user-friendly workflow that is particularly advantageous in clinical settings. Our comprehensive evaluations across

various imaging modalities demonstrate that MedSAM-2 consistently outperforms current state-of-the-art models, offering superior generalization capabilities and robust performance across multiple segmentation tasks.

The implications of this research are profound, suggesting that the use of video segmentation principles in medical imaging can significantly enhance the precision and utility of diagnostic tools. Looking forward, we anticipate further refinements in our approach, particularly in the areas of real-time processing and the integration of more diverse data types. Future work will also explore the potential for MedSAM-2 to be adapted for other complex segmentation scenarios outside the medical field, broadening the scope of this powerful technology.

REFERENCES

- Tumor detection, segmentation and classification challenge on automated 3d breast ultrasound (abus) 2023. <https://tdsc-abus2023.grand-challenge.org>, 20203.
- Cross-modality domain adaptation for medical image segmentation. <https://crossmoda-challenge.ml>, 2023.
- Tomer Amit, Eliya Nachmani, Tal Shaharbany, and Lior Wolf. Segdiff: Image segmentation with diffusion probabilistic models. *arXiv preprint arXiv:2112.00390*, 2021.
- Mehdi Astaraki, Simone Bendazzoli, and Iuliana Toma-Dasu. Fully automatic segmentation of gross target volume and organs-at-risk for radiotherapy planning of nasopharyngeal carcinoma. *arXiv preprint arXiv:2310.02972*, 2023.
- Ujjwal Baid, Satyam Ghodasara, Suyash Mohan, Michel Bilello, Evan Calabrese, Errol Colak, Keyvan Farahani, Jayashree Kalpathy-Cramer, Felipe C Kitamura, Sarthak Pati, et al. The rsna-asnr-miccai brats 2021 benchmark on brain tumor segmentation and radiogenomic classification. *arXiv preprint arXiv:2107.02314*, 2021.
- Federico Bolelli. Tooth fairy: A cone-beam computed tomography segmentation challenge. *International Conference on Medical Image Computing and Computer Assisted Intervention (MICCAI) 2023*, 2023.
- Victor Ion Butoi, Jose Javier Gonzalez Ortiz, Tianyu Ma, Mert R Sabuncu, John Guttag, and Adrian V Dalca. Universeg: Universal medical image segmentation. *arXiv preprint arXiv:2304.06131*, 2023.
- Jieneng Chen, Yongyi Lu, Qihang Yu, Xiangde Luo, Ehsan Adeli, Yan Wang, Le Lu, Alan L Yuille, and Yuyin Zhou. Transunet: Transformers make strong encoders for medical image segmentation. *arXiv preprint arXiv:2102.04306*, 2021.
- Junlong Cheng, Jin Ye, Zhongying Deng, Jianpin Chen, Tianbin Li, Haoyu Wang, Yanzhou Su, Ziyang Huang, Jilong Chen, Lei Jiang, et al. Sam-med2d. *arXiv preprint arXiv:2308.16184*, 2023a.
- Junlong Cheng et al. Sam-med2d. *arXiv preprint arXiv:2308.16184*, 2023b.
- Chen Chu, Jihui Zheng, and Yong Zhou. Ultrasonic thyroid nodule detection method based on u-net network. *Computer Methods and Programs in Biomedicine*, 199:105906, 2021.
- Guoyao Deng et al. Sam-u: Multi-box prompts triggered uncertainty estimation for reliable sam in medical image. *arXiv preprint arXiv:2307.04973*, 2023.
- Yuhang Ding, Xin Yu, and Yi Yang. Modeling the probabilistic distribution of unlabeled data for one-shot medical image segmentation. In *Proceedings of the AAAI conference on artificial intelligence*, volume 35, pp. 1246–1254, 2021.
- Huihui Fang, Fei Li, Huazhu Fu, Xu Sun, Xingxing Cao, Jaemin Son, Shuang Yu, Menglu Zhang, Chenglang Yuan, Cheng Bian, et al. Refuge2 challenge: Treasure for multi-domain learning in glaucoma assessment. *arXiv preprint arXiv:2202.08994*, 2022.
- Xi Fang and Pingkun Yan. Multi-organ segmentation over partially labeled datasets with multi-scale feature abstraction. *IEEE Transactions on Medical Imaging*, 39(11):3619–3629, 2020.
- Haifan Gong, Guanqi Chen, Ranran Wang, Xiang Xie, Mingzhi Mao, Yizhou Yu, Fei Chen, and Guanbin Li. Multi-task learning for thyroid nodule segmentation with thyroid region prior. In *2021 IEEE 18th International Symposium on Biomedical Imaging (ISBI)*, pp. 257–261. IEEE, 2021.
- Ali Hatamizadeh, Vishwesh Nath, Yucheng Tang, Dong Yang, Holger R Roth, and Daguang Xu. Swin unetr: Swin transformers for semantic segmentation of brain tumors in mri images. In *International MICCAI Brainlesion Workshop*, pp. 272–284. Springer, 2022a.
- Ali Hatamizadeh, Yucheng Tang, Vishwesh Nath, Dong Yang, Andriy Myronenko, Bennett Landman, Holger R Roth, and Daguang Xu. Unetr: Transformers for 3d medical image segmentation. In *Proceedings of the IEEE/CVF Winter Conference on Applications of Computer Vision*, pp. 574–584, 2022b.

- Nicholas Heller, Fabian Isensee, Dasha Trofimova, Resha Tejpaul, Zhongchen Zhao, Huai Chen, Lisheng Wang, Alex Golts, Daniel Khapun, Daniel Shats, Yoel Shoshan, Flora Gilboa-Solomon, Yasmeen George, Xi Yang, Jianpeng Zhang, Jing Zhang, Yong Xia, Mengran Wu, Zhiyang Liu, Ed Walczak, Sean McSweeney, Ranveer Vasdev, Chris Hornung, Rafat Solaiman, Jamee Schoephoerster, Bailey Abernathy, David Wu, Safa Abdulkadir, Ben Byun, Justice Spriggs, Griffin Struyk, Alexandra Austin, Ben Simpson, Michael Hagstrom, Sierra Virnig, John French, Nitin Venkatesh, Sarah Chan, Keenan Moore, Anna Jacobsen, Susan Austin, Mark Austin, Subodh Regmi, Nikolaos Papanikolopoulos, and Christopher Weight. The kits21 challenge: Automatic segmentation of kidneys, renal tumors, and renal cysts in corticomedullary-phase ct, 2023.
- AD Hoover, Valentina Kouznetsova, and Michael Goldbaum. Locating blood vessels in retinal images by piecewise threshold probing of a matched filter response. *IEEE Transactions on Medical Imaging*, 19(3):203–210, 2000.
- Fabian Isensee, Paul F Jaeger, Simon AA Kohl, Jens Petersen, and Klaus H Maier-Hein. nnu-net: a self-configuring method for deep learning-based biomedical image segmentation. *Nature methods*, 18(2):203–211, 2021.
- Wei Ji, Shuang Yu, Junde Wu, Kai Ma, Cheng Bian, Qi Bi, Jingjing Li, Hanruo Liu, Li Cheng, and Yefeng Zheng. Learning calibrated medical image segmentation via multi-rater agreement modeling. In *Proceedings of the IEEE/CVF Conference on Computer Vision and Pattern Recognition*, pp. 12341–12351, 2021.
- Alexander Kirillov, Eric Mintun, Nikhila Ravi, Hanzi Mao, Chloe Rolland, Laura Gustafson, Tete Xiao, Spencer Whitehead, Alexander C Berg, Wan-Yen Lo, et al. Segment anything. *arXiv preprint arXiv:2304.02643*, 2023.
- Jinlian Ma, Fa Wu, Tian’an Jiang, Qiyu Zhao, and Dexing Kong. Ultrasound image-based thyroid nodule automatic segmentation using convolutional neural networks. *International journal of computer assisted radiology and surgery*, 12(11):1895–1910, 2017.
- Jun Ma and Bo Wang. Segment anything in medical images. *arXiv preprint arXiv:2304.12306*, 2023.
- Md Ashraful Alam Milton. Automated skin lesion classification using ensemble of deep neural networks in isic 2018: Skin lesion analysis towards melanoma detection challenge. *arXiv preprint arXiv:1901.10802*, 2019.
- Cheng Ouyang, Carlo Biffi, Chen Chen, Turkay Kart, Huaqi Qiu, and Daniel Rueckert. Self-supervision with superpixels: Training few-shot medical image segmentation without annotation. In *Computer Vision—ECCV 2020: 16th European Conference, Glasgow, UK, August 23–28, 2020, Proceedings, Part XXIX 16*, pp. 762–780. Springer, 2020.
- Lina Pedraza, Carlos Vargas, Fabián Narváez, Oscar Durán, Emma Muñoz, and Eduardo Romero. An open access thyroid ultrasound image database. In *10th International Symposium on Medical Information Processing and Analysis*, volume 9287, pp. 92870W. International Society for Optics and Photonics, 2015.
- Cheng Peng, Andriy Myronenko, Ali Hatamizadeh, Vishwesh Nath, Md Mahfuzur Rahman Siddiquee, Yufan He, Daguang Xu, Rama Chellappa, and Dong Yang. Hypersegmas: Bridging one-shot neural architecture search with 3d medical image segmentation using hypernet. In *Proceedings of the IEEE/CVF Conference on Computer Vision and Pattern Recognition*, pp. 20741–20751, 2022.
- Félix Quinton, Romain Popoff, Benoît Presles, Sarah Leclerc, Fabrice Meriaudeau, Guillaume Nodari, Olivier Lopez, Julie Pellegrinelli, Olivier Chevallier, Dominique Ginhac, et al. A tumour and liver automatic segmentation (atlas) dataset on contrast-enhanced magnetic resonance imaging for hepatocellular carcinoma. *Data*, 8(5):79, 2023.
- Nikhila Ravi, Valentin Gabeur, Yuan-Ting Hu, Ronghang Hu, Chaitanya Ryali, Tengyu Ma, Haitham Khedr, Roman Rädle, Chloe Rolland, Laura Gustafson, Eric Mintun, Junting Pan, Kalyan Vasudev Alwala, Nicolas Carion, Chao-Yuan Wu, Ross Girshick, Piotr Dollár, and Christoph Feichtenhofer. Sam 2: Segment anything in images and videos. *arXiv preprint*, 2024.

- Abhijit Guha Roy, Shayan Siddiqui, Sebastian Pölsterl, Nassir Navab, and Christian Wachinger. ‘squeeze & excite’ guided few-shot segmentation of volumetric images. *Medical image analysis*, 59:101587, 2020.
- Saikat Roy, Tassilo Wald, Gregor Koehler, Maximilian R Rokuss, Nico Disch, Julius Holzschuh, David Zimmerer, and Klaus H Maier-Hein. Sam. md: Zero-shot medical image segmentation capabilities of the segment anything model. *arXiv preprint arXiv:2304.05396*, 2023.
- Jiacheng Wang, Lan Wei, Liansheng Wang, Qichao Zhou, Lei Zhu, and Jing Qin. Boundary-aware transformers for skin lesion segmentation. In *Medical Image Computing and Computer Assisted Intervention—MICCAI 2021: 24th International Conference, Strasbourg, France, September 27–October 1, 2021, Proceedings, Part I 24*, pp. 206–216. Springer, 2021a.
- Kaixin Wang, Jun Hao Liew, Yingtian Zou, Daquan Zhou, and Jiashi Feng. Panet: Few-shot image semantic segmentation with prototype alignment. In *proceedings of the IEEE/CVF international conference on computer vision*, pp. 9197–9206, 2019a.
- Lu Wang, Dongxue Liang, Xiaolei Yin, Jing Qiu, Zhiyun Yang, Junhui Xing, Jianzeng Dong, and Zhaoyuan Ma. Coronary artery segmentation in angiographic videos utilizing spatial-temporal information. *BMC medical imaging*, 20:1–10, 2020.
- Shujun Wang, Lequan Yu, Kang Li, Xin Yang, Chi-Wing Fu, and Pheng-Ann Heng. Boundary and entropy-driven adversarial learning for fundus image segmentation. In *International Conference on Medical Image Computing and Computer-Assisted Intervention*, pp. 102–110. Springer, 2019b.
- Wenxuan Wang, Chen Chen, Meng Ding, Hong Yu, Sen Zha, and Jiangyun Li. Transbts: Multimodal brain tumor segmentation using transformer. In *International Conference on Medical Image Computing and Computer-Assisted Intervention*, pp. 109–119. Springer, 2021b.
- Xinlong Wang, Wen Wang, Yue Cao, Chunhua Shen, and Tiejun Huang. Images speak in images: A generalist painter for in-context visual learning. In *Proceedings of the IEEE/CVF Conference on Computer Vision and Pattern Recognition*, pp. 6830–6839, 2023a.
- Xinlong Wang, Xiaosong Zhang, Yue Cao, Wen Wang, Chunhua Shen, and Tiejun Huang. Seggpt: Segmenting everything in context. *arXiv preprint arXiv:2304.03284*, 2023b.
- Jason Wei, Yi Tay, Rishi Bommasani, Colin Raffel, Barret Zoph, Sebastian Borgeaud, Dani Yogatama, Maarten Bosma, Denny Zhou, Donald Metzler, et al. Emergent abilities of large language models. *arXiv preprint arXiv:2206.07682*, 2022.
- Qiaoqiao Wei et al. Focused and collaborative feedback integration for interactive image segmentation. In *CVPR*, pp. 18643–18652, 2023.
- Julia Wolleb, Robin Sandkühler, Florentin Bieder, Philippe Valmaggia, and Philippe C Cattin. Diffusion models for implicit image segmentation ensembles. *arXiv preprint arXiv:2112.03145*, 2021.
- Sanghyun Woo, Shoubhik Debnath, Ronghang Hu, Xinlei Chen, Zhuang Liu, In So Kweon, and Saining Xie. Convnext v2: Co-designing and scaling convnets with masked autoencoders. In *CVPR*, pp. 16133–16142, 2023.
- Huisi Wu, Shihuai Chen, Guilian Chen, Wei Wang, Baiying Lei, and Zhenkun Wen. Fat-net: Feature adaptive transformers for automated skin lesion segmentation. *Medical image analysis*, 76:102327, 2022a.
- Junde Wu and Min Xu. One-prompt to segment all medical images. In *Proceedings of the IEEE/CVF Conference on Computer Vision and Pattern Recognition (CVPR)*, pp. 11302–11312, June 2024.
- Junde Wu, Huihui Fang, Yu Zhang, Yehui Yang, and Yanwu Xu. Medsegdiff: Medical image segmentation with diffusion probabilistic model. *arXiv preprint arXiv:2211.00611*, 2022b.
- Junde Wu, Rao Fu, Huihui Fang, Yuanpei Liu, Zhaowei Wang, Yanwu Xu, Yueming Jin, and Tal Arbel. Medical sam adapter: Adapting segment anything model for medical image segmentation. *arXiv preprint arXiv:2304.12620*, 2023.

- Junde Wu, Wei Ji, Huazhu Fu, Min Xu, Yueming Jin, and Yanwu Xu. Medsegdiff-v2: Diffusion-based medical image segmentation with transformer. In *Proceedings of the AAAI Conference on Artificial Intelligence*, volume 38, pp. 6030–6038, 2024.
- Shuang Yu, Di Xiao, Shaun Frost, and Yogesan Kanagasigam. Robust optic disc and cup segmentation with deep learning for glaucoma detection. *Computerized Medical Imaging and Graphics*, 74: 61–71, 2019.
- Kaidong Zhang et al. Customized segment anything model for medical image segmentation. *arXiv preprint arXiv:2304.13785*, 2023.
- Amy Zhao, Guha Balakrishnan, Fredo Durand, John V Guttag, and Adrian V Dalca. Data augmentation using learned transformations for one-shot medical image segmentation. In *Proceedings of the IEEE/CVF conference on computer vision and pattern recognition*, pp. 8543–8553, 2019.
- Xin Zheng, Yong Wang, Guoyou Wang, and Jianguo Liu. Fast and robust segmentation of white blood cell images by self-supervised learning. *Micron*, 107:55–71, 2018.
- Tianfei Zhou et al. Volumetric memory network for interactive medical image segmentation. *Medical Image Analysis*, 83:102599, 2023.